Measurement of sprinkled and encapsulated space charge in homo-multilayer dielectric samples using PEA method

Marek FLORKOWSKI[ID]* and **Maciej KUNIEWSKI**[ID]

AGH University of Science and Technology, Department of Electrical and Power Engineering, al. Mickiewicza 30, 30-059 Kraków, Poland

Abstract. High voltage DC insulation plays an important role, especially in power transmission systems (HVDC) but also increasingly on medium voltage levels (MVDC). The space charge behavior under DC voltage has great importance on electrical insulation reliability. This paper reports investigations of encapsulated space charge in homo-multilayer dielectric materials using the pulsed electro-acoustic (PEA) method. The charge has been introduced on the homo-layer interface by corona sprinkling prior to encapsulation. Two doses of charge density were accumulated on the dielectric surface in two types of dielectric materials Kapton and LDPE. The polarization DC voltage was applied in 2 min intervals in steps corresponding to an effective electric field strength in a range of 8–40 kV/mm for Kapton and 10–50 kV/mm for LDPE. The PEA-based detected space charge was compared at the initial, reference stage, prior to charge accumulation, and after corona sprinkling of defined charge density. The evaluation was based on the PEA time-dependent charge distributions and charge profiles referring to the DC polarization field strength. The goal of the experiment was to identify the relationship and the character of the known sprinkled and encapsulated charge inside homo-layered materials using the PEA method. According to the observations, the ratio between sprinkled charge densities is proportional to the encapsulated, charge densities measured by the PEA method on the interfacial homo-layer for the Kapton specimen. In the case of LDPE, a fast decrease of interfacial charge was observed, especially at a higher polarization field above 10 kV/mm. The encapsulation of the known charge amount can be extended to different types of multilayer material. The presented methodology might be used also for extended calibration of the PEA measurement system.

Key words: space charge; corona discharge; encapsulated charge; PEA (pulsed electro-acoustic) method; high voltage insulation; diagnostics.

1. INTRODUCTION

The condition of high voltage (HV) insulation is a crucial element of a reliable and resilient electrical power system. High voltage DC insulation plays an important role, especially in HVDC power transmission systems but also increasingly on medium voltage level MVDC. It has also applications in new domains such as e-mobility where the rise in voltage levels is systematically observed. However, one of the main application fields refers to DC cable insulation based on polymeric materials, especially polyethylene. Despite the overall great electrical performance, such materials suffer from the accumulation of the space charge at DC voltage, leading potentially to a dielectric breakdown [1–5]. Among accessories, the cable joints, composed of multilayer materials, are prone to this effect. In addition, temperature variation has serious implications on electric field distribution. The accumulation of space charge in solid dielectrics is an inherent consequence of a non-uniform variation in conductivity throughout the insulation [6–9]. The total electric field strength in the dielectric material is a superposition effect of externally applied voltage and the internally accumulated space charges [10]. For detection and evaluation of em-bedded charge distribution, the pulsed electro-acoustic (PEA) method has gained a lot of attention and reputation over the last decades [11–13]. Special focus is paid to the multi-layer dielectric materials in terms of PEA instrumentation and interpretation of results, including possible misclassifications due to reflections [4, 14]. The corona charge injection in LDPE material and the observation of both surface and bulk charge density using the PEA method were presented in [15]. The influence of the corona discharges on space charge accumulation in polyimide film was shown in [16]. The embedded charge may have a different origin in the dielectric material, i.e. intrinsic but also caused for example by partial discharges [4, 9, 17–21].

This paper reports on investigations of encapsulated space charge in homo-multilayer dielectric materials using the PEA method. The goal of the experiment was to identify the relationship and the character of the known sprinkled and encapsulated charge inside homo-layered materials with an interfacial charge detected by a PEA method.

2. METHODOLOGY OF THE EXPERIMENT

Usually, the PEA method is used to measure and analyze the space charge embedded in the dielectric insulation material, both in terms of intensity and localization. In the presented paper the investigations on an accumulated and embedded charge in a specimen were carried out. The consecutive stages of ex-

Bull. Pol. Acad. Sci. Tech. Sci., vol. 70, no. 2, p. e140686, 2022

1

Marek Florkowski and Maciej Kuniewski

perimental methodology are illustrated in Fig. 1. First, the multilayer sample, consisting of the two homo-layers of the same material, has been measured by the PEA method as a reference case. Then, the initial surface potential measurement was performed. In the following step, the surface of one internal layer (upper side of a bottom layer) has been sprinkled with a charge using a corona approach.
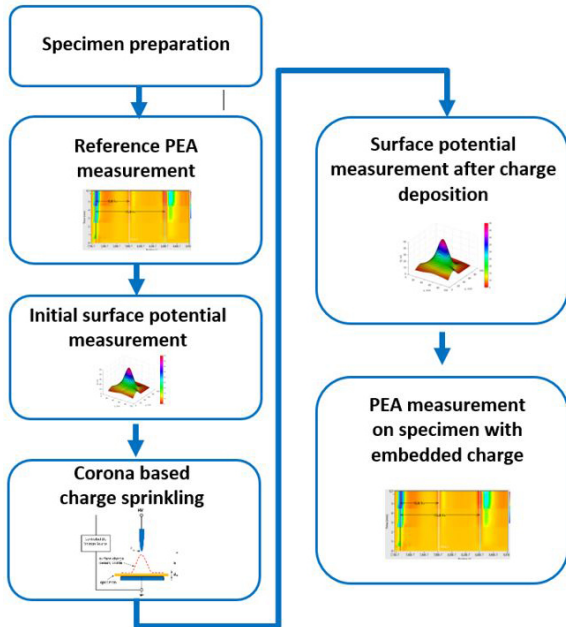

Fig. 1. Consecutive stages of the methodology and experimental sequence

In this way, a space charge with a known average density has been encapsulated inside the homogenous dielectric material on the internal interface layer between two sheets. Immediately after charge deposition, the surface potential was measured on the specimen. The obtained specimen was containing the known density of an accumulated space charge in the precisely spatially defined region. After forming the sandwich specimen the space charge was measured and compared with initial reference values.

3. EXPERIMENTAL SETUP, INSTRUMENTATION AND SPECIMEN

The experimental setup is shown in Fig. 2. The charge sprinkling configuration is presented in Fig. 2a and the PEA instrumentation is shown in Fig. 2b. To inject and embed a charge inside a specimen, a corona-based sparkling is used [15, 22]. The charge was sprinkled applying a DC voltage to a needle (radius of 300 mm) HV electrode placed at a distance of 30 mm above the specimen surface located on the ground planar electrode. The sparkling duration was 5 min. Two doses were obtained at a voltage of 12 kV and 15 kV. The charge density was measured using the system presented in [23] as well as the field-nulling technique for non-contacting voltage measurement using Trek model 347. The charge was accumulated on
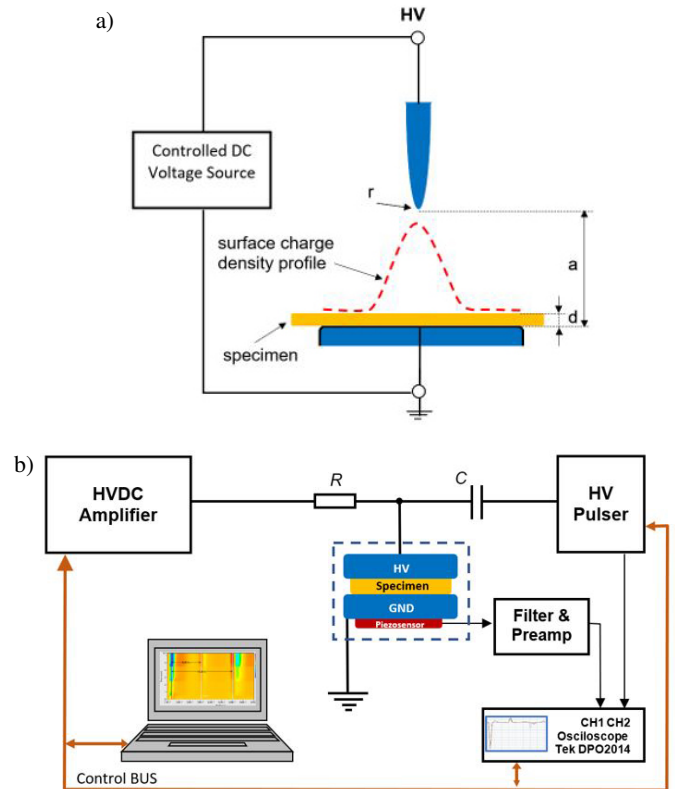

Fig. 2. Experimental set-up for: a) charge sparkling and b) PEA measurement: R – limiting resistor; C – coupling capacitor

one side of the interlayer interface of the specimen. Then the specimen was immediately placed between the aluminum electrodes of the PEA (pulsed electro-acoustic) system. The PVDF (polyvinylidene fluoride) sensor 9 mm thick was installed. The PEA head consists of the DC polarizing voltage and pulse stimuli. The DC voltage is delivered from a high voltage amplifier (Glassman High Voltage Power Supply), whereas the charge vibration impulse is provided by a fast HV pulser. The signal detected at the piezoelectric sensor is filtered, pre-amplified, and acquired using fast sampling 5 GS/s recorder with a bandwidth of 1 GHz. The amplitude of this signal is proportional to the charge embedded in the insulation and spatial position concerning the sensor. In postprocessing, signal-to-noise improvement was achieved by applying averaging over a packet of waveforms.

For the presented measurement the polarization voltage was up to 10 kV, corresponding to the electric field strength in the specimen up to 50 kV/mm depending on the specimen selection. The high voltage DC was applied during the whole measurement time, while the excitation pulse had 5 ns width and 2 kV amplitude and was repeated with a frequency of 100 Hz.

The measurement was performed on two types of specimens: Kapton and LDPE. Kapton belongs to a polyimide family manufactured by DuPont. The one sheet of the Kapton specimen film was 125 mm thick. The LDPE (low-density polyethylene) single slice was 100 mm thick. The measurements were carried out at room temperature 22°C and humidity 37%. The specimen formation sequence is shown in Fig. 3.
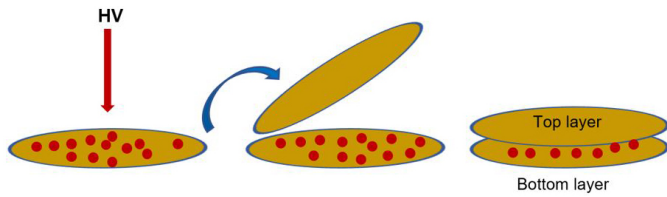
Fig. 3. Formation of the specimen with embedded charge

In order to encapsulate the sprinkled charge, the homo-layered specimen was formed from two similar sheets of dielectric material. Always one, inner bottom-side of the sheet was pre-charged on the interface between the layers.

4. SIGNAL PROCESSING IN THE PEA METHOD

Signal processing is an important step in the PEA method. Not only does it refer to the proper extraction of the acoustic waveforms generated by charges vibration but also to the proper interpretation of the transformed signals concerning the underlying physical phenomena. Even in the case of the homogenous specimen, the superposition of reflected and incident waveforms results in a complex waveform detected by a piezoelectric sensor. The situation is far more complicated in the case of a multilayer sample, as every interlayer interface contributes to another set of waveforms. The exemplary set of the incident and reflected waveforms in the case of two layers specimen is shown in Fig. 4. The interface between Kapton layers is marked by a very tiny machine oil separation to indicate the borderline (the thickness of the layers is not in scale) on the layer diagram (Fig. 4a). The selected individual incident and reflected components of the acoustic wave occurring in the multilayer specimen are shown in Fig. 4b, whereas the resultant waveform is in Fig. 4c. The traveling time in every layer depends on the layer thickness and sound propagation velocity v in the material. The reflections are occurring on the interlayer interface. It is caused by acoustic impedance z transition, defined as $z = \rho \cdot v$, where ρ represents material density [24]. In that context, it is important to separate and extract signals representing the space charge without superimposed reflection components. If two layers have equal properties and thickness the middle waveform magnitude corresponds to the thickness of the coupling interface layer between samples. The thinner the coupling layer the smaller signal at the interface and the less interfered signal corresponding to the HV is observed. The spatial resolution Δx is determined by the signal sampling time Dt and the wave propagation velocity v. Assuming the sampling step equal to 400 ps and the wave propagation velocity $2 \cdot 10^3$ ms^{-1}, the spatial resolution yields $\Delta x = 0.8$ mm. The detected raw signal from a sensor after filtering and amplification performed in the hardware requires several processing steps prior to analysis, implemented usually in the software.

The main blocks, shown in Fig. 5, are related to:
- signal averaging
- digital band-pass filtering
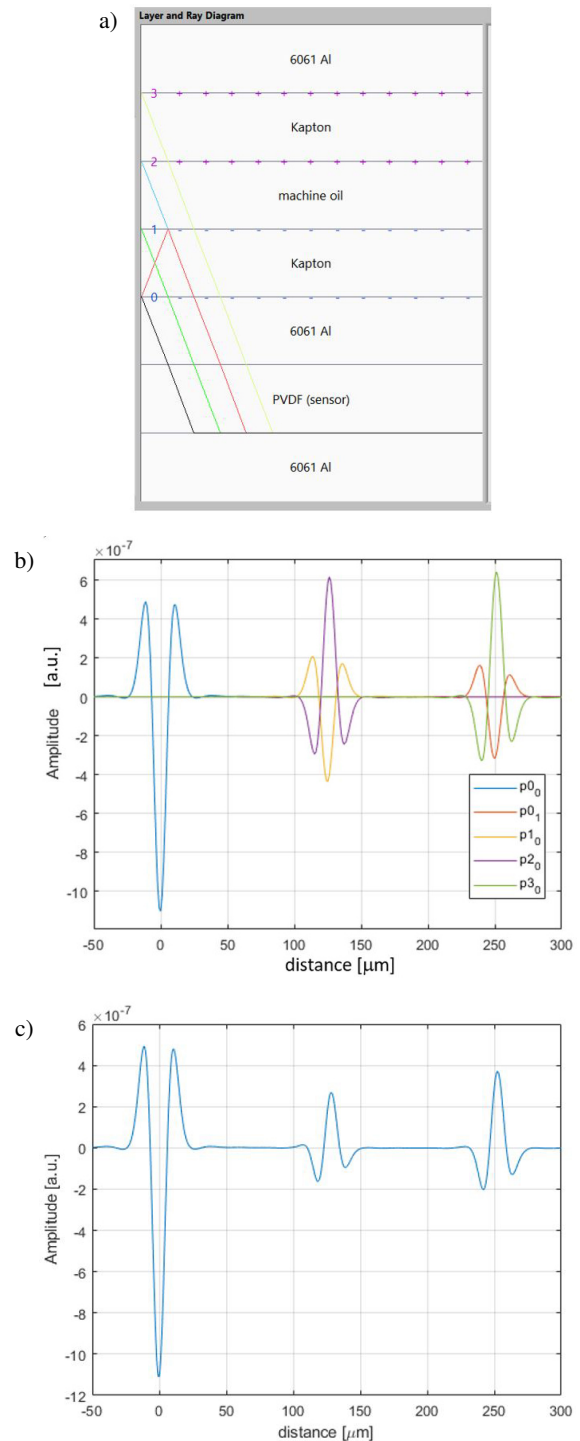- spectrum transformation
- deconvolution

Fig. 4. The superposition of in incident and reflected waveforms in case of two-layer specimen: a) layer reflection diagram; b) individual incident and reflected components of the acoustic wave; c) resultant waveform

The objective of those processing steps is to improve both signal-to-noise ratio (SNR) and spatial resolution.

The applied averaging of 50 signal waveforms resulted in the proportional to the square root of the number of waveforms SNR improvement, i.e. by 7.1. Then the digital filtering is performed in the frequency domain, transforming the signal by fast
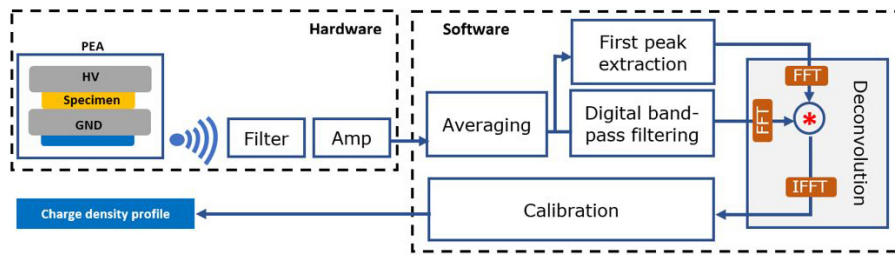
Fig. 5. Signal processing steps in the PEA method

Fourier transform (FFT), applying the sine windowed Gaussian filtering with center frequency f_0 and bandwidth Δf, and then transforming back the signal to the time domain by inverse FFT. The profile of the filter $G(f)$ is described by [25]:

$$G(f) = \exp\left[-A\left(\frac{f-f_0}{\Delta f}\right)^2\right] \cdot \sin\left(B\frac{f}{f_0}\right), \qquad (1)$$

where A, B are constants.

In order to further improve the PEA signal profile dedicated manipulations and transformation might be performed in the frequency domain on the spectrum. The most popular is selective filtering applied using various classes of digital filters. Then, the important step in PEA signal processing is always deconvolution. Since an acquired signal $pea(t)$ is a convolution in the time domain of sensor characteristics $s(t)$ with an original signal $o(t)$ propagating due to charge vibrations. Usually, also a noise component $n(t)$ is considered

$$pea(t) = o(t) \cdot s(t) + n(t). \qquad (2)$$

Then applied is often the Wiener deconvolution approach based on the minimization of the mean square error. However, neglecting the noise impact the direct computation can be used:

$$pea(t) = o(t) \cdot s(t). \qquad (3)$$

To extract the original signal $o(t)$ the deconvolution operation is involved. If there exist Fourier transforms $O(\omega) = F[o(t)]$ and $S(\omega) = F[(s(t)]$ of both signals $o(t)$ and $s(t)$, the above equation can be rewritten in the frequency domain as:

$$PEA(\omega) = O(\omega) \cdot S(\omega). \qquad (4)$$

The system response $s(t)$ is represented often by a first wavelet in the recorded signal, which does not contain the embedded charge signal. Hence, it is extracted and used for further processing. The convolution in the time domain of signal $o(t)$ and $s(t)$ corresponds to spectra multiplication in the frequency domain. Thus after re-arrangements the original signal o(t) has a form:

$$o(t) = F^{-1}\left[\frac{PEA(\omega)}{S(\omega)}\right]. \qquad (5)$$

The last step is related to calibration to convert the measured voltage signal to corresponding charge density values using a calibration factor k. Assuming charge-free specimen, the

charge density σ at the ground electrode in response to the applied voltage U is [12, 26]:

$$\sigma = \varepsilon_0 \varepsilon_r \cdot U_{dc}/d, \qquad (6)$$

where ε_0 is vacuum permittivity, ε_r is material relative permittivity, d is thickness of the specimen.

Denoting V_m the corresponding magnitude of the peak in the $o(t)$ waveform and approximating it with a triangular shape with a half-width τ of the signal one can get the charge density as:

$$\sigma = k \cdot V_m \cdot \tau \cdot S_v, \qquad (7)$$

where S_v is a sound velocity in a specimen.

From above the calibration factor k is defined as:

$$k = \frac{\varepsilon_0 \varepsilon_r U_{dc}}{d \cdot \tau \cdot S_v \cdot V_m}. \qquad (8)$$

After the calibration process, the processed waveform reflects the accumulated charge distribution in the dielectric material.

Since in the presented results both layers are from the same material, the encapsulated charge was positioned on the interface.

5. RESULTS AND DISCUSSION

The charge encapsulation and PEA-based internal charge distribution measurements were performed on two specimens Kapton and LDPE, containing no embedded charge prior to experiments. The goal of the experiment was to identify the relationship and the character of the known sprinkled and encapsulated charge inside homo-layered materials using the PEA method. The polarization DC voltage was applied in 2 min intervals in the following steps: 2 kV, 5 kV, and 10 kV resulting in effective electric field strength equal to 8 kV/mm, 20 kV/mm, and 40 kV/mm for Kapton and 10 kV/mm, 25 kV/mm, and 50 kV/mm for LDPE specimen. The charge vibration excitation pulse had a magnitude of 2 kV, width 5 ns, and repetition frequency of 100 Hz.

It is important to notice that due to the needle-plane configuration, the sprinkled charge has non-uniform surface distribution. In this way, the measured values of surface charge density correspond to the peak position. Whereas in the PEA method the averaged charge density in the layer is obtained. Thus, the intention of this paper is rather to show the relationship between

4

Bull. Pol. Acad. Sci. Tech. Sci., vol. 70, no. 2, p. e140686, 2022

the sprinkled and measured charge, than the direct absolute correspondence. The time-dependent charge distributions in a reference Kapton specimen prior to charge accumulation – and after the charge deposition are shown in Fig. 6. The two sprinkled non-uniform surface charge density doses were accumulated with peak values $\sigma_{1K} = 0.4$ μC/m^2 and $\sigma_{2K} = 0.7$ μC/m^2 in Kapton interlayer. The changing with time electric field stress is marked in Fig. 6a.
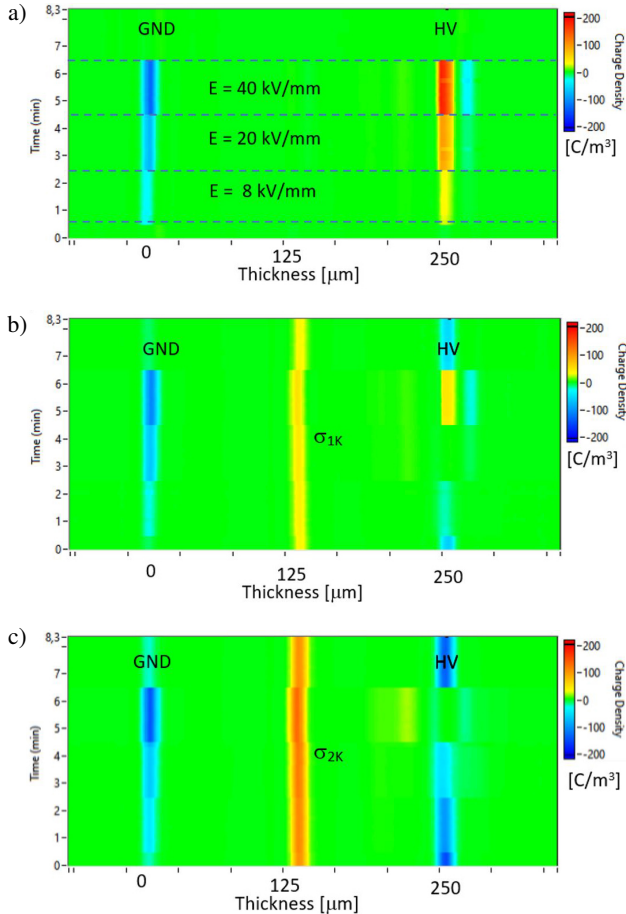

Fig. 6. Time and voltage-dependent space charge distribution in Kapton specimen: a) with no embedded charge, b) with $\sigma_{1K} = 0.4$ μC/m^2 of sprinkled charge density, c) with $\sigma_{2K} = 0.7$ μC/m^2 of sprinkled charge density in the inter homo-layers

The corresponding space charge profiles for the reference case and both encapsulated charge density variants with σ_{1K} and σ_{2K} are presented in Fig. 7. For the charge-free reference case (Figs. 6a and 7a), no interfacial charge is observed. While increasing the voltage, thus polarizing the electric field, the charge density adjacent to electrodes has intensified.

The encapsulated charge of both doses can be clearly recognized in the map views (Figs. 6b, 6c) and in charge distribution profiles in Figs. 7b and 7c.

The measured values of accumulated charge at internal Kapton interface yield, depending on the value of a polarizing field, between 80 C/m^3 and 120 C/m^3 for the encapsulated charge corresponding to σ_{1K}, and between 140 C/m^3 and 180 C/m^3 for sprinkled dose σ_{2K}.

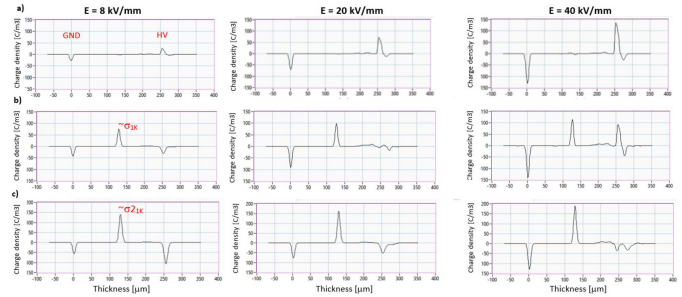**Fig. 7.** Selected space charge profiles in Kapton specimen: a) with no embedded charge, b) with $\sigma_{1K} = 0.4$ μC/m^2 of sprinkled charge density, c) with $\sigma_{2K} = 0.7$ μC/m^2 of sprinkled charge. In each above case, polarization electric field strength was 8 kV/mm, 20 kV/mm, and 40 kV/mm respectively

As can be seen, the relationship between the charge density ratios of the interfacial peak in the above cases is kept constant. The high DC polarization field, varying in the range from 8 kV/mm to 40 kV/mm, is influencing the electrode adjacent charge. On the side of the electrodes is also the visible influence of the induced charge caused by the middle layer embedded charge, being in the superposition with a polarization charge. The sprinkled and encapsulated charge is visible in the specimen throughout the whole experimental sequence and is present also after switching off the polarizing DC field. The ratio between sprinkled charge densities is proportional to the encapsulated, charge densities measured by the PEA method on the interfacial homo-layer.

The second experiment referred to the LDPE homo-layers. Due to the smaller sample thickness, the maximal polarization field is higher, reaching 50 kV/mm, compared with the Kapton specimen. The time-dependent charge distributions in a reference LDPE specimen before charge accumulation – and after the charge deposition are shown in Fig. 8. The two sprinkled charge density doses $\sigma_{1L} = 0.5$ μC/m^2 and $\sigma_{2L} = 0.9$ μC/m^2 were accumulated inside the LDPE specimen. This interfacial encapsulated charge is detected at the lower electric field, i.e. 10, 25 kV/mm (incl. polarization-free state) and disappears at high electric stress 50 kV/mm. The corresponding space charge profiles for the reference case and both encapsulated charge densities are visualized in Fig. 9. For the charge-free reference case (Figs. 8a and 9a), no interfacial charge is observed. While increasing the voltage, the charge density adjacent to electrodes has intensified. The encapsulated charge can be clearly recognized in the middle of the specimen at 10 kV/mm and is diminishing with increasing stress. As can be seen also from the time-voltage map display, the encapsulated charge is not visible anymore after switching off the DC sequence, unlike the Kapton case. The comparison of the encapsulated charge peak values related to σ_{1L} to σ_{2L} is showing a very similar value, not related to the original proportions. This effect may be attributed to the charge decay and transport at the LDPE homo-layer interface. Already after the sprinkling stage, much faster surface potential decay was observed for LDPE specimen (ranging in minutes) compared with Kapton. The charge decay process is influenced also by neutralization in the air
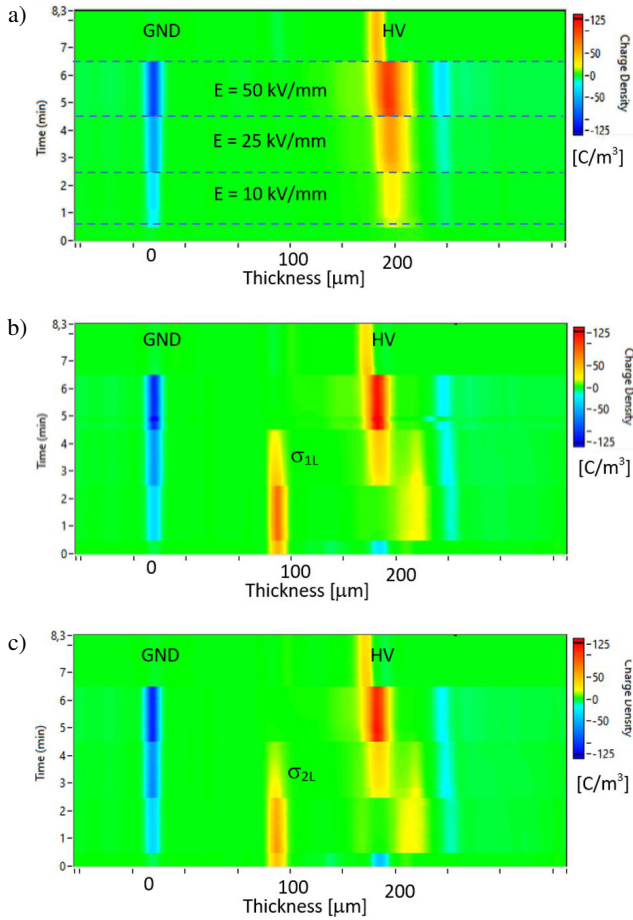
Bull. Pol. Acad. Sci. Tech. Sci., vol. 70, no. 2, p. e140686, 2022

5

Fig. 8. Time and voltage-dependent space charge distribution in LDPE specimen: a) with no embedded charge, b) with $\sigma_{1L} = 0.5$ μC/m^2 of sprinkled charge density, c) with $\sigma_{2L} = 0.9$ μC/m^2 of sprinkled charge density in the inter homo-layers

prior to encapsulation [27–29]. Then, the decay is occurring due to bulk charge transport supported by the DC polarization field.

Interesting observation yields the measurement performed without DC polarization field, only applying the high voltage readout impulse, stimulating the charge vibration. The exemplary charge profiles recorded at charge-free Kapton specimen
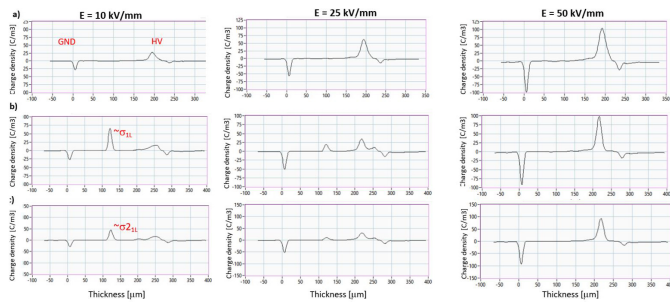

Fig. 9. Selected space charge profiles in LDPE specimen: a) with no embedded charge, b) with $\sigma_{1L} = 0.5$ μC/m^2 of sprinkled charge density, c) with $\sigma_{2L} = 0.9$ μC/m^2 of sprinkled charge. In each case examples for polarization electric field strength 10 kV/mm, 25 kV/mm and 50 kV/mm are shown

and with encapsulated charges with densities σ_{1K} and σ_{2K} are shown in Fig. 10.
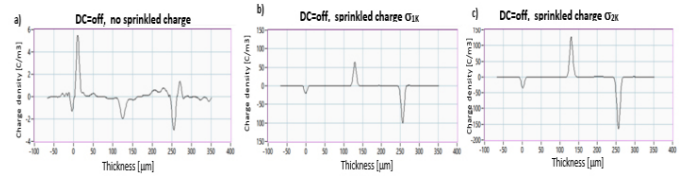

Fig. 10. Space charge profiles in Kapton specimen recorded only at high voltage readout impulse, without DC polarization field: a) interfacial charge-free specimen, b) with sprinkled charge density σ_{1K}, c) and with σ_{2KL}

In case of no externally sprinkled interfacial charge (Fig. 10a), only a tiny residual charge profile is recorded, with a very small magnitude. The introduction of the encapsulated positive charge results in the induction on both electrode sides of the negative charge. The magnitude relation of the detected charge at the homo-layer interface is corresponding to the sprinkled charge density. The time variation and transport of sprinkled, the interfacial charge was not investigated in the scope of this work.

6. CONCLUSIONS

This paper reports on investigations of encapsulated space charge in homo-multilayer dielectric materials using the PEA method. The charge has been introduced on the homo-layer interface by corona sprinkling prior to encapsulation. Two doses of charge density were accumulated on the dielectric surface. The following two types of dielectric materials were analyzed: Kapton and LDPE, comparing the PEA-based detected space charge at the initial, reference stage, prior to charge accumulation, and after corona sprinkling of defined charge density. According to the observations, the ratio between sprinkled charge densities is proportional to the encapsulated, charge densities measured by the PEA method on the interfacial homo-layer for the Kapton specimen. In the case of LDPE, a fast decrease of interfacial charge was observed, especially at higher polarization fields above 10 kV/mm. The encapsulation of the known charge amount can be extended to different types of multilayer material. The presented methodology might be used also for extended calibration of the PEA measurement system.

REFERENCES

[1] Z. Li and B. Du, "Polymeric Insulation for High-Voltage DC Extruded Cables: Challenges and Development Directions," *IEEE Electr. Insul. Mag.*, vol. 34, no. 6, pp. 30–43, 2018, doi: 10.1109/MEI.2018.8507715.

[2] G. Rizzo, P. Romano, A. Imburgia, and G. Ala, "Review of the PEA Method for Space Charge Measurements on HVDC Cables and Mini-Cables," *Energies*, vol. 12, p. 3512, 2019.

[3] T. Tohmine, T. Fujitomi, H. Miyake, Y. Tanaka, Y. Ida, and Y. Inoue, "Measurement of Space Charge Accumulated in Multi-Layered Samples Composed of Different Insulators used in the Joints of DC Transmission Cables," *Proc. of Conference ISEIM*, 2017.

6

Bull. Pol. Acad. Sci. Tech. Sci., vol. 70, no. 2, p. e140686, 2022

[4] T. Takada, T. Tohmine, Y. Tanaka, J. Li, "Space charge accumulation in double-layer dielectric systems—measurement methods and quantum chemical calculations," *IEEE Electr. Insul. Mag.*, vol. 35, no. 5, pp. 36–46, 2019.

[5] M. Florkowski, *Partial discharges in high-voltage insulating systems – mechanisms, processing, and analytics*, AGH Press, Kraków, 2020.

[6] G.M. Sessler, J.E. West, D.A. Berkley, and G. Morgenster, "Determination of Spatial Distribution of Charges in Thin Dielectrics," *Phys. Rev. Lett.*, vol. 38, no. 7, p. 368, 1977.

[7] I.W. McAllister, G.C. Crichton, and A. Pedersen, "Charge Accumulation in DC Cables: A Macroscopic Approach," *IEEE Int. Symp. on Electrical Insulation*, Pittsburgh, USA, 1994.

[8] K. Wu and C. Cheng, "Interface Charges between Insulating Materials," *IEEE Trans. Dielectr. Electr. Insul.*, vol. 24, no. 4, pp. 2633–2642, 2017.

[9] G. Teyssedre, F. Zheng, L. Boudou, and C. Laurent, "Charge trap spectroscopy in polymer dielectrics: a critical review," *J. Phys. D: Appl. Phys.*, vol. 54, p. 263001, 2021.

[10] M. Takashima, K. Soda, and T. Takada, "Measurement of electric charges at the interface between two dielectric layers using an electro-acoustic transducer technique," *IEEE Trans. Dielectr. Electr. Insul.*, vol. 23, no. 2, pp. 287–295, 1988.

[11] T. Takada and T. Sakai, "Measurement of Electric Fields at a Dielectric / Electrode Interface Using an Acoustic Transducer Technique," *IEEE Trans. Dielectr. Electr. Insul.*, vol. EI-18, no. 6, pp. 619–628, 1983.

[12] T. Maeno, "Portable space charge measurement system using the pulsed electroacoustic method," *Proc. 7th Int. Conf. on Properties and Applications of Dielectric Materials*, Nagoya, 2003.

[13] G. Mazzanti, G.C. Montanari, and .M. Alison, "A space charge based method for the estimation of apparent mobility and trap depth as markers for insulation degradation-theoretical basis and experimental validation," *IEEE Trans. Dielectr. Electr. Insul.*, vol. 10, pp. 187–197, 2003.

[14] R. Bogega, P.H.F. Morshuis, and J.J. Smit, "Space Charge Signal Interpretation in a Multi-layer Dielectric Tested by Means of the PEA Method," *Int. Conf \. on Solid Dielectrics*, Toulouse, France, 2004.

[15] G. Chen, "A new model for surface potential decay of corona-charged polymers," *J. Phys. D: Appl. Phys.*, vol. 43, p. 55405, 2010.

[16] T. Kan, K. Abe, H. Miyake, Y. Tanaka, and T. Maeno, "The influence of Corona Discharge on Space Charge Accumulation in Polyimide Film," *IEEE Conf. on Electrical Insulation and Dielectric Phenomena*, 2013.

[17] M. Florkowski, B. Florkowska, M. Kuniewski, and P. Zydroń, "Mapping of Discharge Channels in Void Creating Effective Partial Discharge Area," *IEEE Trans. Dielectr. Electr. Insul.*, vol. 25, no. 6, pp. 2220–2228, 2018.

[18] M. Kunicki, "Variability of the Acoustic Emission Signals Generated by Partial Discharges in Mineral Oil," *Arch. Acoust.*, vol. 44, no. 2, pp. 339–348, 2019.

[19] M. Florkowski, "Influence of Insulating Material Properties on Partial Discharges at DC Voltage," *Energies*, vol. 13, p. 4305, 2020.

[20] C. Pan, K. Wu, G. Chen, M. Florkowski, Z. Lv, and J. Tang, "Understanding Partial Discharge Behavior from the Memory Effect Induced by Residual Charges: A Review," *IEEE Trans. Dielectr. Electr. Insul.*, vol. 27, no. 6, pp. 1936–1950, 2020.

[21] M.A. Saleh, S.S. Refaat, M. Olesz, H. Abu-rub, and J. Guźiński, "The effect of protrusions on the initiation of partial discharges in XLPE high voltage cables," *Bull. Pol. Acad. Sci. Tech. Sci.*, vol. 69, no. 1, p. e136037, 2021.

[22] M. Florkowski, "Imaging and simulations of positive surface and airborne streamers adjacent to dielectric material," *Measurement*, vol. 186, p. 110170, 2021.

[23] M. Florkowski, D. Krześniak, M. Kuniewski, and P. Zydroń, "Surface discharge imaging in presence of deposited space charges in non-uniform electric field at DC voltage," *High Voltage*, special issue "Partial Discharges at DC", vol. 6, pp. 576–589, 2021.

[24] M.A. Andrade *et al.*, "Interpretation of PEA Output Signal in a Multilayer Specimen," *IEEE Conf. on Electrical Insulation and Dielectric Phenomena*, Cancun, Mexico, 2018.

[25] L.H. Pearson, J.R. Dennison, E.W. Griffiths, and A.C. Pearson, "PEA System Modeling and Signal Processing for Measurement of Volume Charge Distributions in Thin Dielectric Films," *IEEE Trans. Plasma Sci.*, vol. 45, no. 8, pp. 1955–1964, 2017.

[26] N. Kirigaya, K. Iguchi, H. Miyake, and Y. Tanaka, "Proposal of Calibration Method for Space Charge Distribution in Laminated Films Using PEA Measurement System," *Int. Symposium on Electrical Insulating Materials (ISEIM)*, 2020.

[27] M. Ieda, G. Sawa, and U. Shinohara, "A Decay Process of Surface Electric Charges across Poyethylene Film," *Jap. J. Appl. Phys. s*, vol. 6, p. 793, 1967.

[28] M. Florkowski, B. Florkowska, and R. Włodek, "Investigations on Post Partial Discharge Charge Decay in Void Using Chopped Sequence," *IEEE Trans. Dielectr. Electr. Insul.*, vol. 26, no. 6, pp. 3831–3838, 2017.

[29] Z. Lei, C. Li, R. Men, and J. He, "Mechanism of bulk charging behavior of ethylene propylene rubber subjected to surface charge accumulation," *J. Appl. Phys.*, vol. 124, p. 244103, 2018.